J Solid State Electrochem (2011) 15:2005–2011
DOI 10.1007/s10008-010-1222-6

ORIGINAL PAPER

Electrochemical capacitance of nickel oxide nanotubes synthesized in anodic aluminum oxide templates

Juan Xu · Lan Gao · Jianyu Cao · Wenchang Wang · Zhidong Chen

Received: 17 July 2010 / Revised: 8 October 2010 / Accepted: 18 October 2010 / Published online: 31 October 2010

Abstract Nickel oxide (NiO) nanotubes for supercapacitors were synthesized by chemically depositing nickel hydroxide in anodic aluminum oxide templates and thermally annealing at 360 °C. The synthesized nanotubes have been characterized by scanning electron microscopy, transmission electron microscopy, and X-ray diffraction. The capacitive behavior of the NiO nanotubes was investigated by cyclic voltammetry, galvanostatic charge–discharge experiment, and electrochemical impedance spectroscopy in 6 M KOH. The electrochemical data demonstrate that the NiO nanotubes display good capacitive behavior with a specific capacitance of 266 Fg^{-1} at a current density of 0.1 Ag^{-1} and excellent specific capacitance retention of ca. 93% after 1,000 continuous charge–discharge cycles, indicating that the NiO nanotubes can become promising electroactive materials for supercapacitor.

Keywords Nickel oxide (NiO) nanotubes · AAO template · Supercapacitors

Introduction

Supercapacitors are important electrical energy storage devices that possess the features of high specific power density, fast charge and discharge rate, and long cycle life [1]. Based on different energy storage mechanism, supercapacitors could be classified into two categories: electric double layer capacitors (EDLCs) and pseudocapacitors. The capacitance of EDLCs is based on charge separation at the electrode/electrolyte interface, whereas the capacitance of pseudocapacitors arises from fast and reversible faradic redox reactions that can occur within the electroactive materials. Among the electroactive materials used for pseudocapacitors, amorphous hydrated RuO_2 has been identified to be an influential material because of its fairly high specific capacitance, good electronic conductivity, and high electrochemical stability [2]. However, the commercial application of RuO_2 was hindered by its high cost and toxicity [3, 4]. Hence, considerable efforts have been devoted to develop alternative electrode materials such as NiO, CoO_x, and MnO_2 [4–9].

With its low cost and environmental friendly nature, NiO has been recognized to be a very promising electrode material for pseudocapacitors [10–15]. Furthermore, recent reports have proved that NiO with special morphology possessed excellent electrochemical capacitive behavior [16]. For example, by using a simple chemical deposition process, Lokhande et al. successfully prepared NiO thin film, which shows a maximum specific capacitance of 167 Fg^{-1} at a potential scan rate of 20 mVs^{-1} [17]. A specific capacitance 710 Fg^{-1} for hierarchical porous NiO was reached by an inexpensive self-assemble method followed by a heat treatment process [10]. Wu et al. prepared aerogel-like mesoporous NiO by sol-gel method with a specific capacitance of 75–125 Fg^{-1} [11]. Zheng et al. reported that the specific capacitance of NiO nanoflake can approximate to 138 Fg^{-1} at a current density of 0.2 Ag^{-1} [18]. Urchin-like NiO synthesized by a hydrothermal process can exhibit a specific capacitance of 217–290 Fg^{-1} [19]. NiO nanotubes have been successfully used as negative electrode materials

J. Xu · L. Gao · J. Cao · W. Wang · Z. Chen (✉)
Jiangsu Polytechnic University,
Changzhou 213164, People's Republic of China
e-mail: cjytion3@163.com

J. Xu · Z. Chen
Qualtec Co. Ltd.,
Changzhou 213164, People's Republic of China

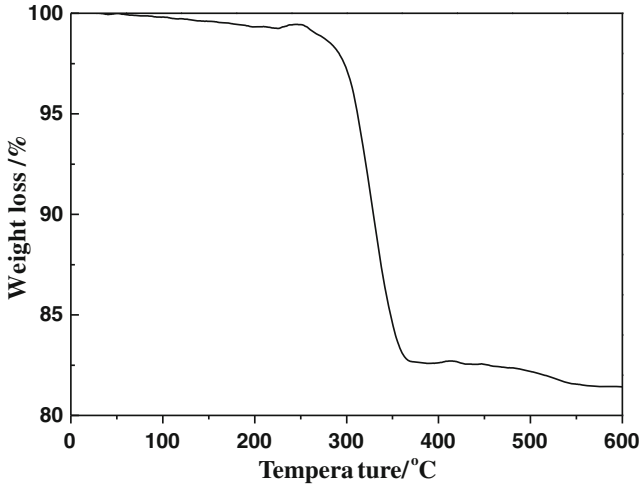

Fig. 1 Thermogravimetric analysis of $Ni(OH)_2$ precursor in N_2 atmosphere

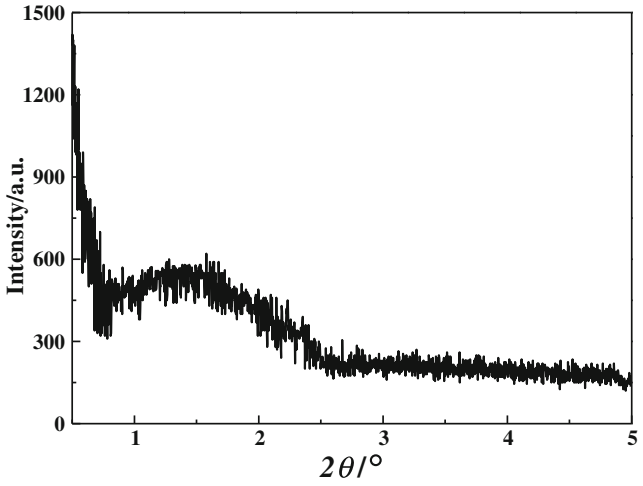

Fig. 3 Low-angle XRD of as-prepared NiO nanotubes

in lithium ion batteries [20] and antimicrobial agents [21]. However, no any attempts have been made to carry on an intensive study of the pseudocapacitive behavior of the one-dimensional NiO nanotubes. Anodic aluminum oxide (AAO) template approach [22] and metal organic chemical vapor deposition (MOCVD) template route [23] have been adopted to prepare the 1D NiO nanotubes. Compared to the MOCVD template route, chemical deposition of metal ions in AAO template is more efficient and feasible because of its unique structural properties, such as well-controlled diameter and height, extremely narrow pore size distribution, and ideally cylindrical pore shape [24]. Herein, NiO nanotubes prepared via the AAO template method have been employed as electroactive materials for supercapacitors and their capacitive behavior was investigated in 6 M KOH electrolyte solution by way of cyclic voltammetry (CV), galvanostatic charge–discharge tests, and electrochemical impedance spectroscopy.

Experimental

Synthesis of NiO nanotubes

For the synthesis of NiO nanotubes, the porous AAO membranes (Whatman Anodisc TM 47) with a pore diameter of 200 nm and a thickness of 60 μm were used

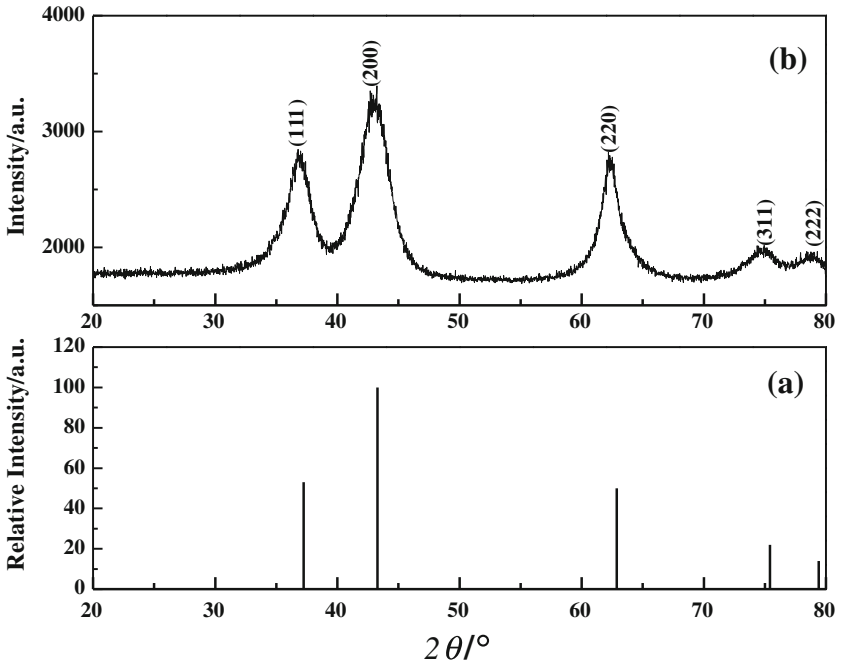

Fig. 2 XRD patterns of standard spectrum (**a**) and as-prepared NiO nanotubes (**b**)

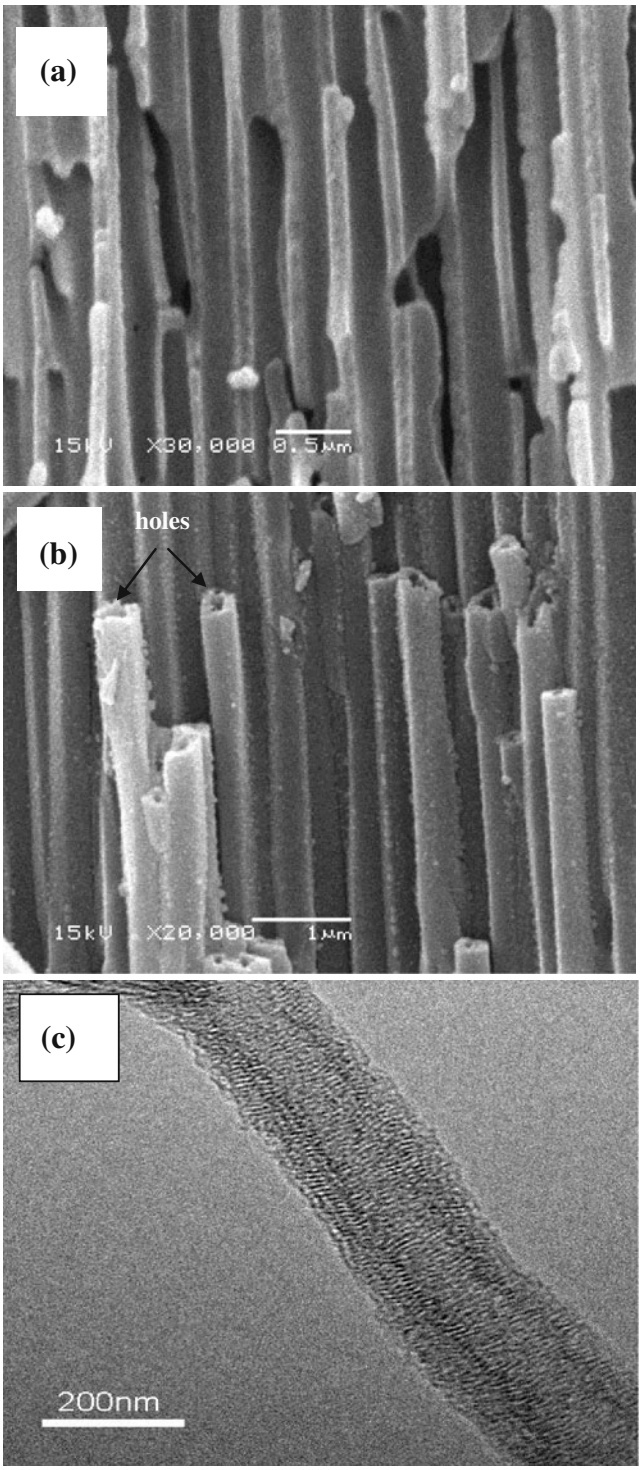

Fig. 4 SEM images of vacant AAO template (**a**), as-prepared NiO nanotubes embedded in an AAO template (**b**), and TEM image of an individual NiO nanotube (**c**)

as the template. The AAO template membranes were immersed in 2 M $NiCl_2$ solution for about 4 h, ensuring that the pores of the template were fully filled with the $NiCl_2$ solution by capillarity force. Then the AAO template was dipped into 1 M NH_4OH solution for 1 h and blue Ni $(OH)_2$ precipitates gradually formed in the pores of the template [25]. After the sample was rinsed with distilled water for several times, it was dried in air at 60 °C for 5 h. Subsequently, the resultant $Ni(OH)_2$ precursors embedded in the AAO template were heated from room temperature to 360 °C in 160 min and maintained for 2 h in the air. This was followed by naturally cooling to room temperature to obtain the NiO nanotubes. Finally, the prepared NiO nanotube bundles were released by thoroughly dissolving the AAO template in 3 M NaOH solution for 5 h.

Structural and morphology characterization

The structure of the as-prepared samples was determined by powder X-ray diffraction (XRD, Rigaku D/max 2500 PC) using Cu Kα radiation. The morphology of the samples was observed by scanning electron microscopy (SEM, JSM-6360LA) and transmission electron microscopy (TEM, Philips Tecnai G2 F20). The nitrogen isotherm was obtained at liquid nitrogen temperature by using a Micromeritics ASAP 2010 apparatus (static volumetric technique). Barrett–Joyner–Halenda (BJH) method, based on the Kelvin equation, was applied to evaluate pore size distribution by desorption branch.

Electrode preparation and electrochemical characterization

The electrode of NiO nanotubes was prepared according to the following steps. Typically, 75% NiO nanotubes powder, 20% acetylene black as a conducting agent, and 5% polytetrafluorethylene as a binder were homogeneously mixed and pressed into a nickel foam (1×1 cm) current collector under a pressure of 8 MPa.

All electrochemical measurements were carried out at room temperature in a three-electrode system consisting of the NiO nanotubes electrode as working electrode, a saturated calomel electrode (SCE, Hg/Hg_2Cl_2) as reference electrode, and a platinum plate (1×1 cm) as counter electrode. The used electrolyte was 6 M KOH solution.

The electrochemical behavior of the NiO nanotubes electrode was characterized by cyclic voltammetry, galvanostatic charge–discharge tests, and electrochemical impedance spectroscopy at VersaSTAT3 electrochemical workstation (Princeton Applied Research, USA). The CV was conducted in a potential range between 0.00 and 0.60 V versus SCE at various scan rates. The constant current charge–discharge tests were carried out at different currents within a potential range of −0.1–0.4 V. Electrochemical impedance spectroscopy was carried out to prove the capacitive performance at open circuit potential in 6 M KOH with a frequency range of $0.01–10^5$ Hz.

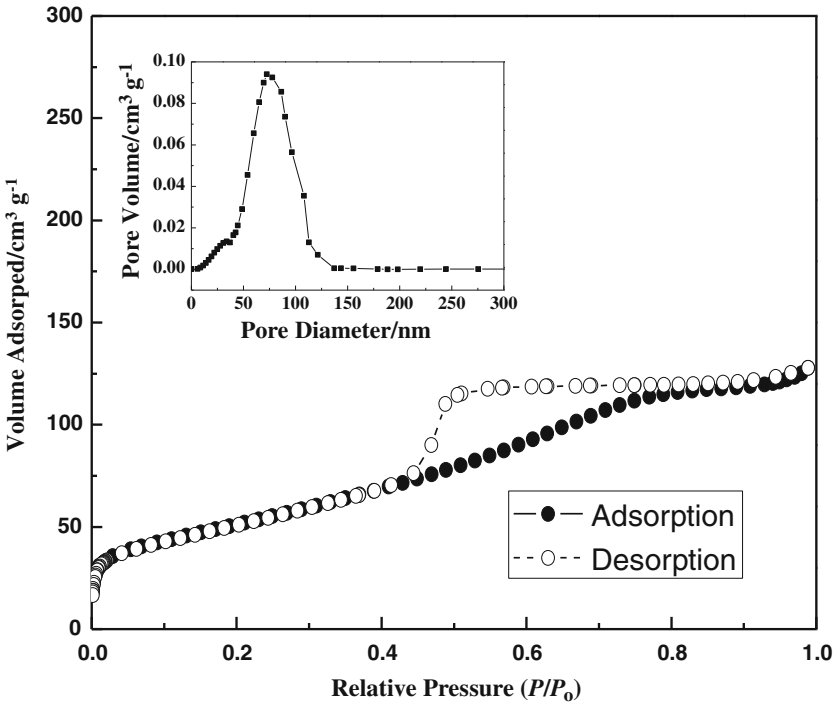

Fig. 5 Nitrogen adsorption/desorption isotherm of as-prepared NiO nanotube. The *inset* shows Barrett-Joyner-Halenda pore size distribution

Results and discussion

Structure analysis and morphology

Thermogravimetric analysis of $Ni(OH)_2$ precursor embedded in AAO template from 0 to 600 °C is shown in Fig. 1. A weight loss of 19.3% from 200 to 360 °C corresponds to the conversion of the $Ni(OH)_2$ to NiO (theoretically, 19.4%).

As shown in Fig. 2, all diffraction peaks of the as-prepared sample were indexed undisputedly to cubic NiO as confirmed from the standard data (JCPDS 47-1049). The diffraction peaks at 37.18, 43.24, 62.76, 75.34, and 79.40° can be respectively denoted as 111, 200, 220, 311, and 222 reflections and the broad peaks indicate that the overall morphology of the as-prepared NiO is nanocrystalline [11]. XRD measurements confirmed that NiO were obtained by the thermal decomposition of $Ni(OH)_2$ precursor at 360 °C.

The low-angle XRD pattern for as-prepared NiO sample is given in Fig. 3. A broad peak can be seen at ca. 1.62°, and the corresponding *d* value for the diffraction angle is 7.8 nm. This value fit well with the pore size obtained from N_2 adsorption measurement, which we will discuss later.

In order to investigate the morphology of the as-prepared sample, the sample embedded in AAO template and that released from the AAO template were characterized by SEM

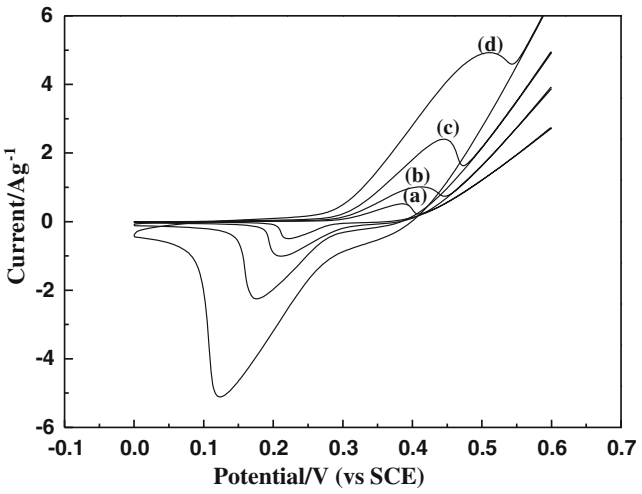

Fig. 6 Cyclic voltammogrames behavior of NiO nanotubes in 6 M KOH electrolyte at various scan rates of 2 mVs^{-1} (*a*), 5 mVs^{-1} (*b*), 10 mVs^{-1} (*c*), and 20 mVs^{-1} (*d*)

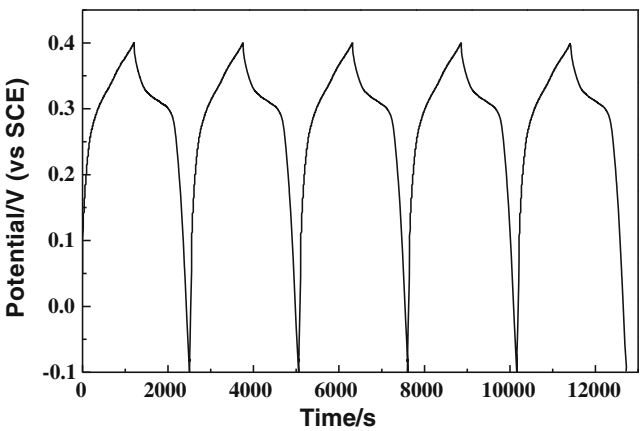

Fig. 7 Galvanostatic charge–discharge curves of NiO nanotubes in 6 M KOH solution at 0.1 Ag^{-1}

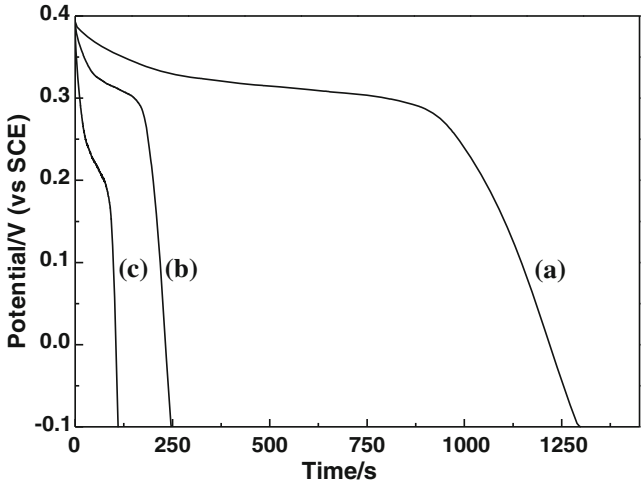

Fig. 8 Galvanostatic discharge curves of NiO nanotubes in 6 M KOH solution at 0.1 Ag^{-1} (*a*), 0.5 Ag^{-1} (*b*), and 1 Ag^{-1} (*c*)

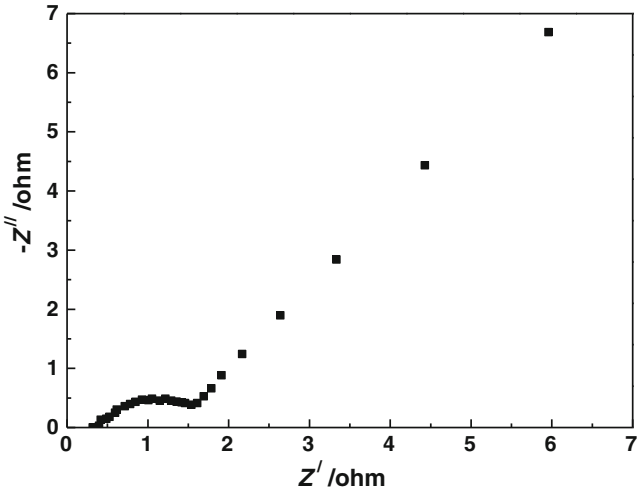

Fig. 10 Impedance plot of NiO nanotube electrode

and TEM, as shown in Fig. 4. Compared with a vacant AAO template (Fig. 4a), the pores of the as-treated AAO template were fully filled with tubular shaped materials after the synthesis process of NiO nanotubes (Fig. 4b), which can be clearly seen from the holes at the broken ends of the fillers. The morphology of individual NiO nanotube indicates that the as-prepared NiO nanotube is about 200 nm in diameters and 40 nm in thickness (Fig. 4c), which were mainly controlled by the pore size of the AAO template and experimental conditions.

Brunaur–Emmett–Teller result shows that the specific surface area of the as-prepared NiO nanotubes is ca. 239 m^2g^{-1} (N_2 adsorption–desorption isotherm was shown in Fig. 5), which is much larger than that of NiO nanoparticles [8], NiO nanoflakes [20], and mesoporous NiO [25]. The BJH pore sizes of the as-prepared NiO nanotubes are in the range of 6–132 nm, indicating that the pores of the NiO nanotubes are mainly mesopores and macropores.

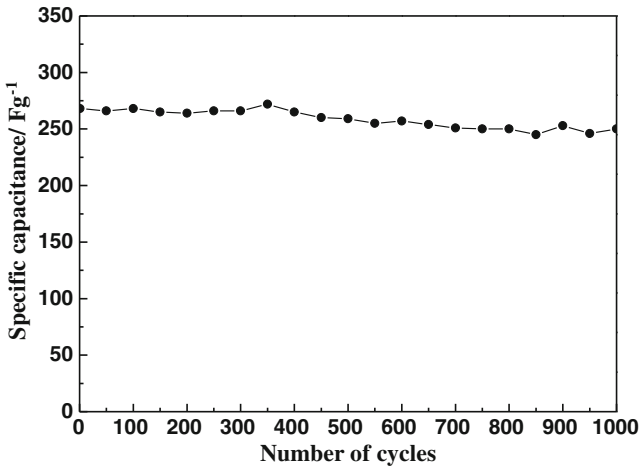

Fig. 9 Dependence of specific capacitance of NiO nanotubes on the number of cycles at 0.1 Ag^{-1}

Cyclic voltammograms

Cyclic voltammetric measurements (CV) were performed in a potential range between 0.00 and 0.60 V (versus SCE) to examine the electrochemical characteristics of the prepared NiO nanotubes electrode. Figure 6 presents the CV curves of the NiO nanotubes electrode in 6 M KOH at different scan rates. A pair of well-defined redox reaction peaks is visible in the CV curves, indicating that the electrochemical capacitance of the NiO nanotubes electrode mainly results from the pseudocapacitance. Furthermore, the peak current increases with increasing scan rate from 2 to 20 mVs^{-1}, which suggests its good reversibility of fast charge–discharge response. In the present study, the pseudocapacitance of NiO in KOH solution is based on the redox process of NiOOH/NiO [11]. Furthermore, the redox reaction peak potential difference of the NiO nanotubes electrode is smaller than that of mesoporous NiO [11], NiO thin film [17], and urchin-like NiO [19] at a same scan rate, which reveals that the electrochemical reversibility of the NiO nanotube electrode is excellent.

Galvanostatic charge–discharge analysis

Figure 7 shows the initial five galvanostatic charge–discharge curves of the NiO nanotubes electrode in 6 M KOH solution at a galvanostatic current density of 0.1 A g^{-1}. The discharge time is approximately equal to the charge time, which represents high discharge efficiency. Moreover, the discharge curve consists of two sections: a sharp decrease of potential followed by a slow drop of potential. This is attributable to the high interfacial

resistance and slow ion transport at the interface between the NiO nanotube electrode and the KOH electrolyte [5].

The specific capacitance has been calculated from the following equation [5, 19]:

$$C = \frac{I \times \Delta t}{\Delta V \times m}$$

Where C ($\mathrm{F\,g^{-1}}$) represents the specific capacitance, I (A) is the galvanostatic current used for charge/discharge, Δt (s) is the time elapsed for the discharge cycle, ΔV (V) is the voltage interval of the discharge, and m (g) is the weight of the active material within the electrode. The specific capacitance of the NiO nanotube electrode determined from the discharge curves is ca. 266 $\mathrm{F\,g^{-1}}$ at a current density of 0.1 $\mathrm{A\,g^{-1}}$, which is much higher than the values of mesoporous NiO [11], NiO nanoflake [18], and NiO nanoparticles [26]. The excellent electrochemical capacitance of the synthesized NiO nanotubes electrode can be attributed to their unique morphology and large specific surface area, which help to enlarge the contact area between electrode and electrolyte and improve the surface adsorption–desorption process of alkali cations.

It is critical for supercapacitor to maintain large capacitances under high charge/discharge current densities because it directly determines its application prospect. Figure 8 shows the galvanostatic charge–discharge curves of the NiO nanotubes electrode in 6 M KOH electrolyte at various galvanostatic current densities. The specific capacitances calculated from each discharge curve in Fig. 8 were 266, 250, and 232 $\mathrm{F\,g^{-1}}$ at 0.1, 0.5, and 1 $\mathrm{A\,g^{-1}}$, respectively. At low current densities, the ohmic drop is low and the inner active sites of the NiO nanotube electrode can be fully utilized, which contribute to achieve high specific capacitance. Due to the comparatively slow rate of redox reactions at high current densities, the specific capacitance decreases with increasing current density [27]. Importantly, compared to the specific capacitance at 0.1 $\mathrm{A\,g^{-1}}$, the value of the NiO nanotube electrode at 1 $\mathrm{A\,g^{-1}}$ only decreases by 17%. The small capacitance fading at a very high galvanostatic current density shows that such a novel nanotube structure allows for a rapid redox reaction at high current densities.

Galvanostatic cycling experiments were undertaken to investigate the cycling stability of the NiO nanotubes electrode. The charge–discharge studies were performed at a current density of 0.1 $\mathrm{A\,g^{-1}}$ in 6 M KOH solution and the variation of specific capacitance for 1,000 cycles is shown in Fig. 9. The NiO nanotube electrode exhibited good stability and reversibility with cycling efficiency of 93% after 1,000 cycles.

Electrochemical impedance spectroscopy analysis

The typical Nyquist plots of NiO nanotubes electrode is presented in Fig. 10. The plot consists of a semicircle at high-frequency region and a straight line at low-frequency region. From the point intersecting with the real axis in the range of high frequency, the internal resistance of the NiO electrode in an open circuit condition is evaluated to be ca. 0.3 Ω, which is composed of three sections [28]: the ionic resistance of electrolyte, the intrinsic resistance of the electro active material, and the contact resistance between the active material and the current collector. In the high-to-medium frequency region, one semicircle related to faradic reactions can be discovered, which should be attributed to the charge transfer resistance at the electrode/electrolyte interface [29, 30]. The phase angle for the impedance plot of the NiO nanotube electrode was observed to be higher than 45° in the low frequencies, suggesting that the electrochemical capacitive behavior of the NiO nanotube electrode is not controlled by diffusion process. These findings imply that the unique structure of the NiO nanotube electrode can facilitate ionic motion in solid electrode.

Conclusions

NiO nanotubes with an outer wall diameter of 200 nm and a wall thickness of 40 nm were used as electroactive materials for supercapacitor. Electrochemical measurements indicated that the as-prepared material could deliver a maximum specific capacitance of 266 $\mathrm{F\,g^{-1}}$ and good stability over 1,000 cycles. Furthermore, high specific capacitance was maintained at high charge/discharge current density due to the unique structure and large surface area of the NiO nanotube electrode. The excellent electrochemical performance coupled with the low cost and simple preparation process render NiO nanotube very promising for practical application in supercapacitors.

Acknowledgment The authors gratefully acknowledge financial support from the National Science Foundation of China (21003015), the Natural Science Foundation of Jiangsu Province (BK2008543), and the Fine Petroleum Chemical Key Laboratories Foundation of Jiangsu Province (KF0701).

References

1. Rajeswari J, Kishore PS, Viswanathan B, Varadarajan TK (2009) Electrochem Commun 11:572
2. Lee BJ, Sivakkumar SR, Ko JM, Kim JH, Jo SM, Kim DY (2007) J Power Sources 168:546
3. Lin YS, Lee KY, Chen KY, Huang YS (2009) Appl Surf Sci 256:1042
4. Liu Y, Zhao WW, Zhang XG (2008) Electrochim Acta 53:3296
5. Gao YY, Chen SL, Cao DX (2010) J Power Sources 195:1757
6. Jiang R, Huang T, Liu J, Zhuang J, Yu A (2009) Electrochim Acta 54:3047
7. Ko JM, Kim KM (2009) Mater Chem Phys 114:837

8. Lee JY, Liang K (2005) Synth Met 150:153
9. Cheng J, Yang YS (2006) J Power Sources 159:734
10. Yuan CZ, Zhang XG, Su LH, Gao B, Shen LF (2009) J Mater Chem 19:5772
11. Wu MQ, Gao JH, Zhang SR, Chen A (2006) J Porous Mater 13:407
12. Wu MS, Huang YA, Yang CH (2008) J Electrochem Soc 11:798
13. Zheng YZ, Zhang ML (2007) Mater Lett 61:3967
14. Wu MS, Hsieh HH (2008) Electrochim Acta 53:2699
15. Nam SH, Kim YS, Shim HS (2008) J Nanosci Nanotechno 8:5427
16. Zhou HH, Chen H, Luo SL (2005) J Solid State Electrochem 9:574
17. Patil UM, Salukhe RR, Gurav KV, Lokhande CD (2008) Appl Surf Sci 255:2603
18. Zheng YZ, Ding HY, Zhang ML (2009) Mater Res Bull 44:403
19. Liu XM, Zhang XG, Fu SY (2006) Mater Res Bull 41:620
20. Needham SA, Wang GX, Liu HK (2006) J Power Sources 159:254
21. Pang H, Lu Q, Li Y, Gao F (2009) Chem Commun 48:7542
22. Shi C, Wang G, Zhao N, Du X, Li J (2008) Chem Phys Lett 454:75
23. Malandrino G, Perdicaro LMS, Fragala IL, Nigro RL, Losurdo M, Bruno G (2007) J Phys Chem C 111:3211
24. Qu X, Dai J, Tian J, Huang X, Liu Z, Shen Z, Wang P (2009) J Alloy Compd 469:332
25. Wang YG, Xia YY (2006) Electrochim Acta 51:3223
26. Ahmad T, Ramanujachary KV, Lofland SE, Ganguli AK (2006) Solid State Sci 8:425
27. Morishita T, Soneda Y, Hatori H, Inagaki M (2007) Electrochim Acta 52:2478
28. Luo JM, Gao B, Zhang XG (2008) Mater Res Bull 43:1119
29. Yuan A, Zhang Q (2006) Electrochem Commun 8:1173
30. Cui L, Li J, Zhang XG (2009) J Appl Electrochem 39:1871